Catalysts **2015**, *5*, 1872-1896; doi:10.3390/catal5041872

OPEN ACCESS

catalysts

ISSN 2073-4344

www.mdpi.com/journal/catalysts

Article

Hydrogen Production by Steam Reforming of Ethanol on Rh-Pt Catalysts: Influence of CeO_2, ZrO_2, and La_2O_3 as Supports

Bernay Cifuentes [1], Manuel F. Valero [1], Juan A. Conesa [2] and Martha Cobo [1,*]

[1] Energy, Materials and Environment Laboratory, Department of Chemical Engineering, Universidad de La Sabana, Campus Universitario Puente del Común, Km. 7 Autopista Norte, Bogotá 250001, Colombia; E-Mails: bernayciva@unisabana.edu.co (B.C.); manuel.valero@unisabana.edu.co (M.F.V.)

[2] Department of Chemical Engineering, Universidad de Alicante, P.O. Box 99, Alicante E-03080, Spain; E-Mail: ja.conesa@ua.es

***** Author to whom correspondence should be addressed; E-Mail: martha.cobo@unisabana.edu.co; Tel./Fax: +57-1-861-5555 (ext. 25207).

Academic Editor: Keith Hohn

Received: 7 October 2015 / Accepted: 2 November 2015 / Published: 11 November 2015

Abstract: CeO_2-, ZrO_2-, and La_2O_3-supported Rh-Pt catalysts were tested to assess their ability to catalyze the steam reforming of ethanol (SRE) for H_2 production. SRE activity tests were performed using $EtOH:H_2O:N_2$ (molar ratio 1:3:51) at a gaseous space velocity of 70,600 h^{-1} between 400 and 700 °C at atmospheric pressure. The SRE stability of the catalysts was tested at 700 °C for 27 h time on stream under the same conditions. $RhPt/CeO_2$, which showed the best performance in the stability test, also produced the highest H_2 yield above 600 °C, followed by $RhPt/La_2O_3$ and $RhPt/ZrO_2$. The fresh and aged catalysts were characterized by TEM, XPS, and TGA. The higher H_2 selectivity of $RhPt/CeO_2$ was ascribed to the formation of small (~5 nm) and stable particles probably consistent of Rh-Pt alloys with a Pt surface enrichment. Both metals were oxidized and acted as an almost constant active phase during the stability test owing to strong metal-support interactions, as well as the superior oxygen mobility of the support. The TGA results confirmed the absence of carbonaceous residues in all the aged catalysts.

Keywords: basic supports; ethanol; hydrogen; Rh-Pt catalyst; steam reforming

1. Introduction

The growing awareness of environmental and energy issues has led to a search for alternative energy sources. Hydrogen, which produces electricity and heat with a high efficiency in fuel cells, is a clean energy source with a higher energy density (141.6 kJ/g) than hydrocarbon fuels [1]. Bioethanol, produced from biomass resources, is an environmentally-sustainable feedstock and, thus, an excellent candidate for industrial-scale hydrogen production through the steam reforming process [2]. Therefore, many countries have invested in bioethanol production. For example, Colombia (South America) has made large investments in bioethanol production via sugar cane fermentation. The bioethanol produced in this way (50 vol % ethanol after flash separation) could be transformed into H_2 by steam reforming for subsequent use in fuel cells.

Steam reforming of ethanol (SRE) for hydrogen production is an endothermic process; Equation (1) gives a simplified representation of this process [3,4]. The SRE can also be represented by a network of reactions (Equations (2)–(10)) [5–7], depending on the reaction conditions and the catalyst used, to reflect the formation of a complex set of by-products including carbon monoxide (CO), methane (CH_4), ethane (C_2H_6), ethylene (C_2H_4), and acetaldehyde (CH_3CHO) [4,8,9].

$$CH_3CH_2OH + 3\,H_2O \rightarrow 2\,CO_2 + 6\,H_2 \quad \Delta H^{o}_{298\,K} = 174\ \text{kJ/mol} \tag{1}$$

$$CO + H_2O \rightleftharpoons CO_2 + H_2 \quad \Delta H^{o}_{298\,K} = -41\ \text{kJ/mol} \tag{2}$$

$$H_3CH_2OH \rightleftharpoons CH_3CHO + H_2 \tag{3}$$

$$CH_3CH_2OH \rightleftharpoons CH_4 + CO + H_2 \tag{4}$$

$$CH_3CHO \rightleftharpoons CH_4 + CO \tag{5}$$

$$CH_4 + H_2O \rightleftharpoons CO + 3H_2 \tag{6}$$

$$CH_3CHO + H_2O \rightleftharpoons CH_4 + CO_2 + H_2 \tag{7}$$

$$CH_3CH_2OH \rightleftharpoons C_2H_4 + H_2O \tag{8}$$

$$C_2H_4 + 2H_2 \rightleftharpoons 2CH_4 \tag{9}$$

$$C_2H_4 + 2H_2O \rightleftharpoons CH_4 + CO_2 + 2H_2 \tag{10}$$

Among these reactions, one of the most important is the water gas shift reaction (WGSR, Equation (2)), which favors CO_2 formation with increasing H_2 and decreasing CO concentrations in the outlet stream [5]. For low-temperature proton exchange membrane fuel cell (PEMFC) applications, a low CO concentration (<100 ppm) is required. The by-product formation, including CO, CH_4, C_2H_4, C_2H_6, and carbon deposits, should be minimized to maximize H_2 production.

The ability of base metals, such as Ni [5,7,10,11], Cu [3,7], Al [12], Zn [13], and Co [14–17], and noble metals, such as Pt [18], Rh [19–22], Pd [23], Ru [24], and Ir [25], supported on various metal oxides to catalyze the SRE has been widely investigated. Ethanol activation pathways depend on the metal nature, and can be generally divided in two groups: the less-oxophilic metals (Pd and Pt) in which α-C–H activation takes place, and the more-oxophilic metals (Co, Ni, Rh, Ru) that promote activation via O–H. Despite its higher cost, noble metals are the best catalyst candidates for SRE due to their greater ability to break C–C bonds, requiring less active metal loading compared to non-noble metals [26].

Likewise, the use of bimetallic catalysts is a strategic option to modify the electronic properties of metal surfaces [27]. By allowing less- and more-oxophilic metals it could be expected changes in the catalytic properties, probably obtaining a more active and resistance catalyst. This is going to be important when real bioethanol samples will be reformed, in which some impurities can weaken catalyst performance [28]. Among the noble metals, Pt and Rh exhibited high activity for breaking the ethanol C–C bond and achieving catalytic WGS conversion, respectively [29,30]. Hence, a very resistant catalyst might be expected.

However, in addition to the catalyst itself, the catalyst support could also influence the activity and stability of the catalyst [31]. Due to the low metal loading when using noble metals (typically < 1%), the direct participation of the support on the reaction mechanism is favored [27]. As was recently pointed out by Zanchet *et al.* [27] in the case of SRE, one point of common agreement is that the oxygen mobility of the support (OSC) is a critical property to favor C removal and avoid deactivation. Thus, higher oxygen storage capacity and oxygen mobility, allow a more effective gasification/oxidation of adsorbed carbon on the surface. These properties can be conferred by reducible supports such as CeO_2, ZrO_2, and La_2O_3 [32]. Among them, cerium oxides have been proposed as catalytically active components for the SRE because of their high oxygen mobility, ability to promote ethanol and water dissociation, ability to disperse metal catalytic components, and strong metal-support interactions that can minimize metal particle sintering [22,33,34]. Favorable reducibility and thermal stability make zirconium oxides potential candidates for catalyst supports [35,36]. Similarly, lanthanum oxides were investigated as promising supports because of their thermal stability and diverse crystalline phases [6,30]. Nevertheless, despite the efforts undertaken to understand the structure and properties of supported bimetallic catalysts, there is a broad set of variables that could be deeply explored concerning the specific conditions of SRE. Catalyst deactivation and the loss of catalytic activity and/or selectivity over time are of great and continuing concern in hydrogen production from ethanol. Regardless of the metal and support used, stability remains a challenge for catalyst design in ethanol reforming [37].

This study aimed to identify an active and stable catalyst that enables the use of the SRE for hydrogen production, for its further use in raw bioethanol samples. For this purpose, a bimetallic 0.6%Rh–0.2%Pt catalyst supported on CeO_2, ZrO_2, or La_2O_3 was selected as a potential catalytic material. Comparing these three supports under the same reaction conditions under kinetic control allowed the selection of the most promising RhPt bimetallic catalyst for further development. A stoichiometric steam/ethanol (S/E) mole ratio of three was employed in all experiments to simulate the bioethanol concentration after flash separating in the commercial samples procured from Colombia and to avoid the presence of dilution effects by water excess [38]. The catalysts were characterized using various techniques, including thermogravimetric analysis (TGA), transmission electron microscopy (TEM), and X-ray photoelectron spectroscopy (XPS). Both reduced and aged catalysts were analyzed to gain some insight into the catalytic mechanism.

2. Results and Discussion

2.1. Catalytic Activity and Selectivity of Reduced Catalysts

Catalytic activity tests were conducted from 400 to 700 °C for both reduced (R) and aged (A) RhPt/CeO_2, RhPt/ZrO_2, and RhPt/La_2O_3, avoiding as much as possible, mass transfer limitations in the

system by the use of an elevated gas hourly space velocity (GHSV) [39]. In addition, the stoichiometric S/E = 3 was employed to simulate bioethanol samples after flash separation. Despite higher water contents increase the thermodynamic favorability to hydrogen production [30], the dilution effects by the water excess can increase the energy consumption [38], which is undesirable to larger scale operations. On the contrary, sub-stoichiometric ratios (S/E < 3) increase coke formation [38]. Hence, S/E = 3 was selected as adequate to test the catalysts.

Figure 1a shows the ethanol conversion by the reduced catalysts and the blank as a function of temperature. No important differences in catalytic activity were observed between the blank test with the empty reactor and those in the presence of only the supports, and total conversion occurred above 600 °C. The blank test produced 0.81 mol H_2/mol ethanol inlet at 700 °C (Figure 1b), consistent with the dominance of decomposition reactions instead ethanol reforming in the absence of a catalyst [40,41].

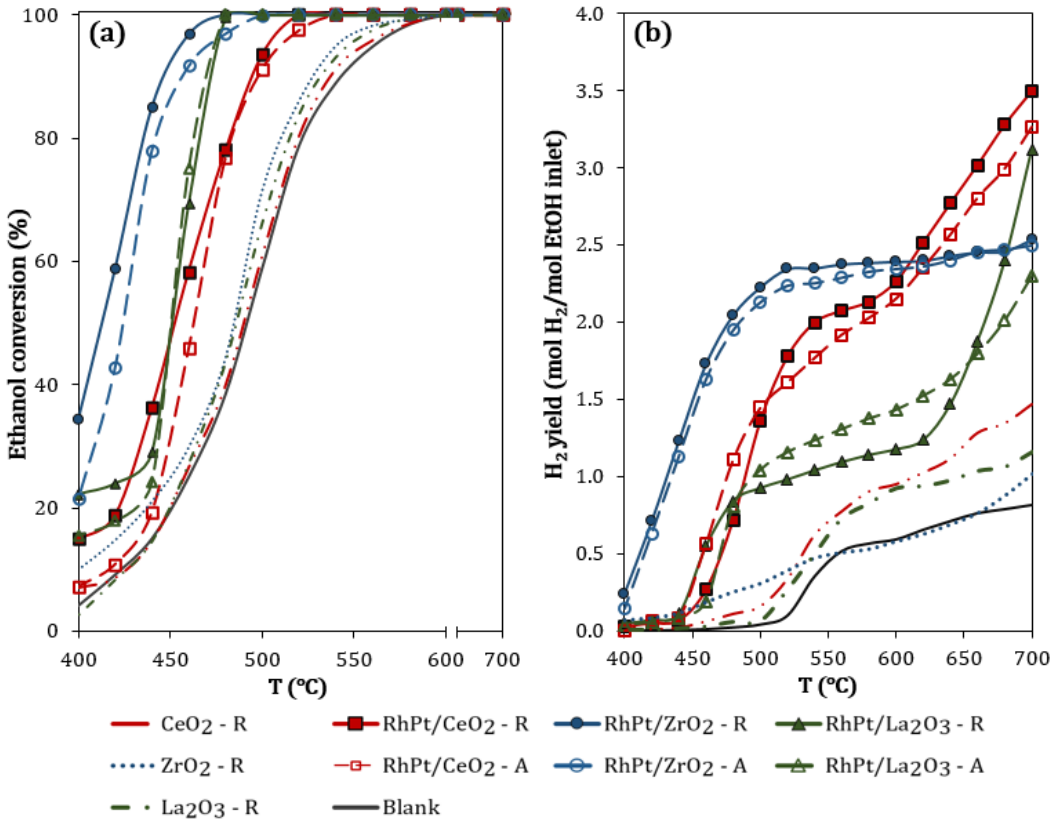

Figure 1. (**a**) Ethanol conversion (XEtOH) and (**b**) H_2 yield as a function of temperature for reduced (R) and aged (A) RhPt/CeO_2, RhPt/ZrO_2, and RhPt/La_2O_3. Reaction conditions: S/E = 3 and GHSV = 70600 h^{-1}. Aged samples obtained after 27 h TOS at 700 °C.

Regarding the supports, CeO_2 and La_2O_3 showed higher H_2 yield compared to ZrO_2 above 500 °C. Table 1 shows the distributions of the main products (H_2, CO, and CO_2) and by-products (CH_4 and ethylene) in the outlet stream at 700 °C (total ethanol conversion conditions) for the different catalyst samples. Acid-basic properties, reducibility, and oxygen storage capacity of the supports are intrinsic characteristics related to the catalytic performance [27]. Acid sites in the support could promote ethanol dehydration to ethylene (Equation (8)). In contrast, basic sites and high oxygen electronic polarizability of the support are favorable for the dehydrogenation (Equation (3)) [37]. Although ceria, zirconia, and

lanthana are recognized as basic supports, they might promote different SRE mechanisms alone and in combination with Rh-Pt active metals. In general, the supports produced H_2, CH_4, and CO_2, which can be related to the occurrence of hydrogenation/dehydrogenation reactions from the adsorbed ethoxy-species. *O*-vacancies present in CeO_2-R favored the dehydration reaction (Equation (7)) through C–O cleavage, preventing the diffusion of C_2 intermediates (like ethylene) [37], and stabilizing hydroxyl groups [27]. However, the lower amounts of H_2 and CO compared with the catalysts shows that the supports are unable to further reform CH_4 (Equation (6)), which is a more stable intermediate [27].

Table 1. Products distribution, catalyst mean active particle size, and carbon deposition in the SRE at 700 °C over reduced (R) and aged (A) $RhPt/CeO_2$, $RhPt/ZrO_2$, and $RhPt/La_2O_3$.

Catalyst Sample	Product Distribution [1]					d_p (nm) [2]	Total Weight Loss (%) [3]
	H_2	CO	CO_2	CH_4	Ethylene		
Equilibrium	0.70	0.24	0.02	N.D.	5E-10	-	-
CeO_2-R	0.52	0.17	0.18	0.12	1E-5	-	0.2
$RhPt/CeO_2$-R	0.70	0.20	0.09	0.01	N.D.	4.6 ± 1.3	0.1
$RhPt/CeO_2$-A	0.65	0.26	0.06	0.03	8E-4	4.8 ± 1.5	0.2
ZrO_2-R	0.46	0.20	0.20	0.14	3E-4	-	0.2
$RhPt/ZrO_2$-R	0.62	0.25	0.10	0.03	7E-5	3.6 ± 1.1	0.2
$RhPt/ZrO_2$-A	0.61	0.26	0.06	0.04	6E-5	9.1 ± 2.4	0.1
La_2O_3-R	0.51	0.17	0.16	0.15	1E-4	-	6.3
$RhPt/La_2O_3$-R	0.66	0.28	0.05	N.D.	N.D.	6.2 ± 2.0	13.4
$RhPt/La_2O_3$-A	0.60	0.35	0.04	N.D.	7E-3	10.0 ± 2.8	13.3

[1] Reaction conditions as Figure 1; [2] Obtained from TEM; [3] From TGA. N.D.: Not detected.

CeO_2 was the most selective support toward H_2 (Figure 1b), probably because it produces larger amounts of acetaldehyde that are subsequently reformed by Equation (7). Hou *et al.* [37] proposed that the reaction mechanism over CeO_2 and Ir/CeO_2 catalysts is: ethanol→ethoxy species→acetaldehyde→ C_2 species→C_1 species. Ethoxy species could be dehydrogenated to acetaldehyde by the presence of –OH groups on the surface of the CeO_2. Carbonate species was only observed in Ir/CeO_2. CeO_2 support oxidizes ethanol into acetaldehyde-acetate species, providing –OH groups and mobile oxygen to ensure the cracking of the C_2 intermediates species and coke cleaning [42]. Likewise, Zanchet *et al.* [27] reported that the conversion of ethanol to ethylene decreases in CeO_2 at high temperature (>250 °C) due to the rise in the energy barriers to dehydration and stability of ethoxy intermediates, thus, dehydrogenation and decomposition reaction take place. ZrO_2 and La_2O_3 showed larger amounts of ethylene than CeO_2, which could result from a major contribution from the dehydration of ethanol (Equation (8)) instead of the dehydrogenation reactions. This phenomenon can be ascribe to a lower oxygen storage capacity of these supports at 700 °C compared with CeO_2 [43,44], which could cause a failure to degrade C_2 intermediates.

Regarding the reduced catalysts, $RhPt/La_2O_3$ and $RhPt/ZrO_2$ achieved complete ethanol conversion above 480 °C (Figure 1a). Unlike these catalysts, $RhPt/CeO_2$ did not achieve complete conversion below 520 °C. Based on the extent of ethanol conversion, the activity order was $RhPt/ZrO_2$ > $RhPt/La_2O_3$ > $RhPt/CeO_2$. The corresponding H_2 yields of the reduced catalysts as a function of temperature are shown in Figure 1b. Above 600 °C, $RhPt/CeO_2$ had the highest yield among the reduced catalysts, with a

maximum of 3.5 mol H_2/mol ethanol inlet at 700 °C. The highest H_2 yield was observed for RhPt/La_2O_3 at 700 °C (3.1 mol H_2/mol ethanol inlet). The yields achieved with both RhPt/CeO_2 and RhPt/La_2O_3 showed significant temperature dependences. In contrast, the behavior of RhPt/ZrO_2 was almost constant between 520 and 700 °C, producing 2.4 mol H_2/mol ethanol inlet. Thus, although RhPt/ZrO_2 was the most active catalyst for converting ethanol at low temperatures, it produced the lowest amount of H_2 under total ethanol conversion conditions at high temperatures.

In this way, the elevated H_2 yield at high temperatures on RhPt/CeO_2 (Figure 1b) could be related to rapid ethanol reforming via dehydrogenation (Equation (3)). The ethanol activation can be occurring over both, Rh via O–H, and Pt via α-C−H, going through the formation of intermediates, such as CH_3C^*O, $^*CH_2C^*O$, and $^*CHC^*O$ [27], where (*) means the chemical bond between the intermediate and the catalyst surface. The cleavage of C–C bond is expected to be favored in species highly dehydrogenated. After the cleavage of C–C bond, $^*CH_x$ and *CO species are formed (Equations (4)–(7)) and, finally, the $^*CH_x$ species are decomposed forming *C that has been oxidized to CO (Equation (6)). The CH_4 selectivity is governed by the ability of the metals to hydrogenate/dehydrogenate the $^*CH_x$ species, that is favored in highly-reduced metals such as Rh [45]. An increase of metal surface reactivity is expected from Pt, that favors H abstraction and increases the availability of O* on the metal surface [27]. In this way, some of the CO produced is converted to CO_2 by the WGSR, which, as expected by thermodynamics, occurred to a lesser extent as the temperature increased (Table 1). Idriss *et al.* [19] and Divins *et al.* [46] evaluated RhPd/CeO_2 catalysts in the SRE, reporting that the increase in H_2 yield around 700 °C is due to simultaneous presence of WGSR and methane reforming.

Additionally, as was analyzed above, the support affects the product distribution in the SRE. Scarabello *et al.* [47] reported that the *O*-vacancy in Rh/Ce-ZrO_2 promotes the oxidation of CO to CO_2 by Equation (11). This reaction is favorable at high temperature because it is endothermic. The occurrence of the two reactions (Equations (2) and (11)) simultaneously could explain the product distribution in RhPt/CeO_2.

$$2CeO_2 + CO \rightleftharpoons CO_2 + Ce_2O_3 \quad (11)$$

In contrast, the stable and limited H_2 yield on RhPt/ZrO_2 at high temperatures (Figure 1b), accompanied by the larger methane production (Table 1), can be associated with ethanol dehydration (Equation (8)) and subsequent ethylene transformation into methane (Equations (9) and (10)). Similar results were reported by Song *et al.* [17], where a Co/ZrO_2 catalyst produced more CH_4 and less CO compared to Co/CeO_2 catalyst under same condition (550 °C, S/E = 10, and GHSV = 5000 h^{-1}). The authors emphasize the high capacity to ZrO_2 to adsorb CO on its surface. Furthermore, previous studies have associated high CH_4 concentrations with the inability of a catalyst to reform methane at high temperatures [30,48]. Martono and Vohs [49] found that the stabilization of Co particles in a partially oxidized form allows bifunctional mechanisms in which oxidative dehydrogenation of ethanol adsorbed on the Co takes place using oxygen supplied by the support. This effect was not observed in non-reducible supports, such as YSZ, due to its low oxygen mobility. Hence, the lack of oxygen vacancies in our ZrO_2, compared to CeO_2, increased CH_4 production [29,43].

The rapid increase in the H_2 yield with temperature, as observed for RhPt/La_2O_3 (Figure 1b), combined with an increase in CO and the absence of CH_4, suggests the reactions represented by

Equations (3)–(6) occur rapidly with temperature [45]. Munera *et al.* [50] proposed a reaction scheme (Equations (12)–(14)) with metallic site (S) and support for the reforming of methane with CO_2 over Rh/La_2O_3. Likewise, Ghelamallah and Granger [51] reported that the increased temperature favored the consumption of H_2 to produce CO, over a $RhPt/La_2O_3$ reduced catalyst in the methane reforming, due to an increasing contribution from the RWGSR (Equation (2)), especially when Pt is present. According to this, CO formation and CH_4 reforming are favored at high temperatures over La_2O_3-supported catalysts, which is consistent with the results obtained in this work.

$$CH_4 + S \rightleftharpoons 2H_2 + S - C \quad (12)$$

$$CO_2 + La_2O_3 \rightleftharpoons La_2O_2CO_3 \quad (13)$$

$$La_2O_2CO_3 + S - C \rightarrow La_2O_3 + CO \quad (14)$$

2.2. Catalyst Stability

The stability of the $RhPt/CeO_2$, $RhPt/ZrO_2$, and $RhPt/La_2O_3$ reduced catalysts was evaluated by 27 h TOS at 700 °C. This temperature was selected to maximize H_2 production and simultaneously decrease methane and ethylene formation. The ethanol conversion and product distribution *vs.* TOS are shown in Figure 2.

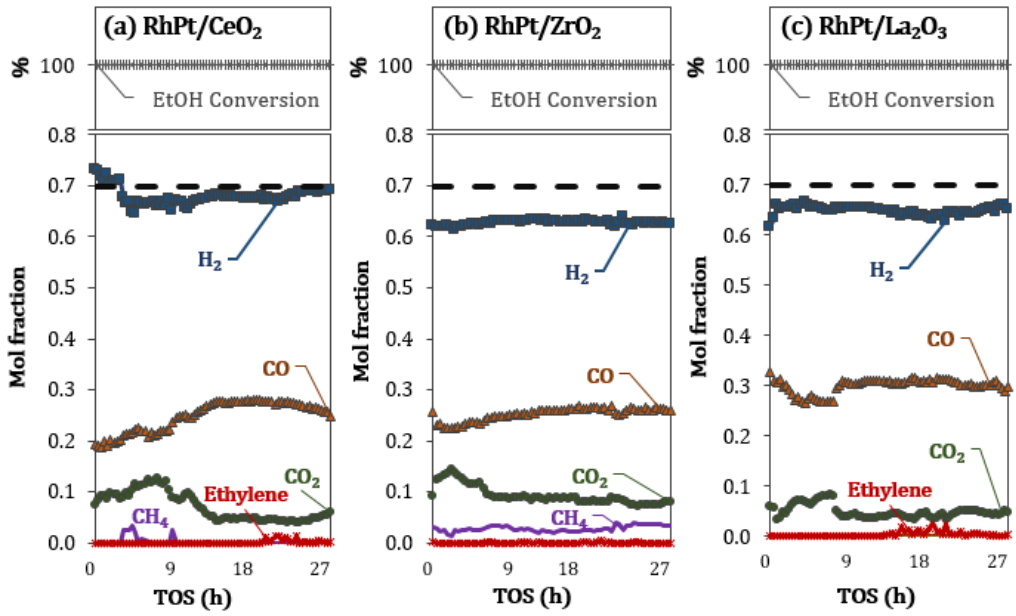

Figure 2. Product distribution (H_2, CO, CO_2, CH_4, and ethylene) as a function of time on stream (TOS) on reduced (**a**) $RhPt/CeO_2$; (**b**) $RhPt/ZrO_2$; and (**c**) $RhPt/La_2O_3$. Dashed line: H_2 equilibrium. Reaction conditions: S/E = 3 and GHSV = 70,600 h^{-1} at 700 °C.

During the tests, all the catalysts showed the same total ethanol conversion without a reduction in catalytic activity, but had different product distributions. Initially, a high H_2 concentration, slightly above the thermodynamic prediction (dashed line), was observed on $RhPt/CeO_2$ (Figure 2a). However, a decrease in the H_2 concentration was observed during the first 5 h, followed by a gradual return to the thermodynamic value. After 27 h TOS, the H_2 concentration was 69 mol%, yielding 3.3 mol H_2/mol ethanol inlet. The H_2 concentration on $RhPt/ZrO_2$ was stable and ~63 mol% H_2 was produced throughout

the experiment (Figure 2b). $RhPt/La_2O_3$ (Figure 2c) showed increased H_2 production until stabilization was observed around 64 mol%. Da Silva *et al.* [44] reported a stable product distribution during total ethanol conversion on $0.6\%Rh/La_2O_3$-SiO_2 and $0.6\%Rh/CeO_2$ catalysts for the SRE during 28 h TOS (500 °C; H_2O:ethanol, molar ratio 3:1; 2.5% ethanol; 30 mL/min gas stream). In the current study, the total gas feed and temperature were extreme, looking forward to affecting the catalyst stability faster, in order to see possible differences between the supported catalysts.

During the first 10 h TOS on $RhPt/CeO_2$, while the H_2 concentration was decreasing, CH_4 was observed (Figure 2a), showing a reduction in the catalyst capacity for methane reforming. After 15 h TOS, the formation of all the products started to stabilize. Some ethylene was sporadically observed after 20 h TOS. $RhPt/ZrO_2$ showed a more stable profile, but methane production was almost constant and higher than that obtained with the other two supports. No methane was detected when $RhPt/La_2O_3$ was used, but some ethylene was observed after 15 h TOS. For all the catalysts, the CO and CO_2 profiles varied with TOS and required more time to stabilize. Thus, the changes undergone by the catalysts with TOS seem to mostly affect the CH_x species dehydrogenation/hydrogenation, the activation of water, and oxidation of *C species [27,52]. Scarabello *et al.* [47] reported that a Rh/ZrO_2 catalyst needed 11 oxidation/reduction cycles to achieve a stable state to reform methane, while Rh/CeO_2-ZrO_2 showed stability without redox cycles, even a low temperature. This phenomenon was associated to changes in the catalyst particle size, dispersion of the active metal, and redistribution of oxygen vacancies in the support surface after each cycle. In addition, Beretta *et al.* [53] proposed that this conditioning period was necessary to remove defect sites on Rh/AlO_2 catalysts in the reforming of methane.

In this study, ethanol conversion and H_2 selectivity did not vary considerably during the stability tests. The most important differences between the reduced and aged catalysts were the changes in the CO and CO_2 distributions with TOS. From this point, we wanted to see the performance of these aged catalysts during the activity test (conversion *vs.* temperature), as the main indicator of catalyst deactivation.

2.3. Catalytic Activity and Selectivity of Aged Catalysts

The aged catalysts after 27 h TOS at 700 °C were investigated for potential loss of activity by performing an activity test (conversion *vs.* temperature). The ethanol conversions and H_2 yield are shown in Figure 1. Compared with the reduced samples, a slight decrease in the activity of the aged catalysts was observed at low temperatures (Figure 1a), but the profile was maintained, suggesting that aging does not alter porous diffusion and the reaction is still kinetic controlled [39,54]. Reduced and aged $RhPt/CeO_2$ and $RhPt/ZrO_2$ had very similar H_2 yield profiles (Figure 1b), but a larger reduction in the H_2 yield was observed for $RhPt/La_2O_3$ at high temperatures. At 700 °C, the H_2 yield followed the trend $RhPt/CeO_2 > RhPt/ZrO_2 > RhPt/La_2O_3$.

In addition, the byproduct distribution at 700 °C (Table 1) of aged catalysts showed an increase in CO and the appearance of ethylene. Again, changes on catalysts performance seems to be associated to CH_x species dehydrogenation/hydrogenation, activation of water, and oxidation of *C species. These steps of the reaction mechanism are structure sensitive [27], which could suggest that the catalysts are suffering changes on particle size and oxidation state. Therefore, the catalytic properties related to active metal dispersion, the oxidation states of the species, and carbon deposition were analyzed to

determine the changes experienced by the materials during the stability tests and relate them to the observed changes in activity.

2.4. Catalyst Characterization

The development of stable catalysts is one of the most important issues in hydrogen production from ethanol, particularly for stoichiometric feed compositions with no excess H_2O to remove carbon deposits [37], as being expected in real bioethanol samples obtained in Colombia. Four intrinsic deactivation modes have been identified: (i) coke formation; (ii) active metal sintering; (iii) active metal oxidation; and (iv) poisoning. Here, catalyst reducibility, TEM, XPS, and TGA were employed to study catalyst deactivation.

2.4.1. Reducibility of Fresh Catalysts

Fresh $RhPt/CeO_2$, $RhPt/ZrO_2$, and $RhPt/La_2O_3$ catalysts and their supports were exposed to a reducing and oxidizing environment periodically at programmed temperatures ranging from 150 to 750 °C in TGA. As shown in Figure 3 (a, c, e for fresh catalysts and b, d, f for supports), the sample was first oxidized at 150 °C (No. 1), then reduced at 150 °C (No. 2), and subsequently heated in inert gas (N_2) until 250 °C. This procedure was repeated each 100 °C until 750 °C.

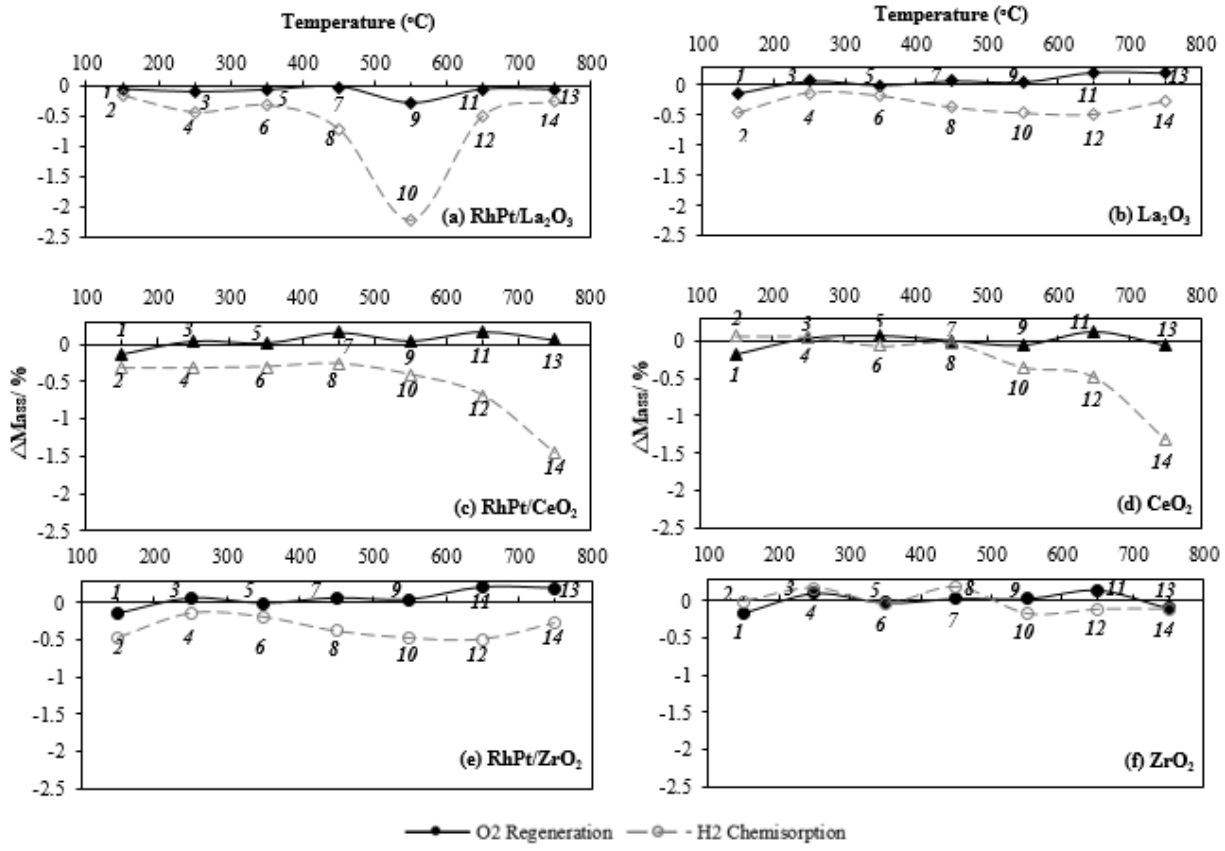

Figure 3. Oxidation in $1\%O_2/N_2$ (No. 1, 3, 5, 7, 9, 11, 13) and reduction in $4\%H_2/N_2$ (No. 2, 4, 6, 8, 10, 12, 14) as a function of temperature in a thermogravimetric analysis of fresh RhPt supported catalysts (**a**, **c**, **e**) and catalyst supports (**b**, **d**, **f**).

The redox properties of the three supports differed (Figure 3b,d,f). In general, the hydrogen flow produced a weight decrease probably as a result of the removal of transferable or fixed oxygen from the support surface by the reaction with H_2 to form water. Conversely, oxygen flow produced mostly a slight increase in weight due to its absorption onto the material surface. ZrO_2 (Figure 3f) was the most stable support, maintaining almost constant weight when exposed to either H_2 or O_2 flow. On the other hand, both La_2O_3 (Figure 3b) and CeO_2 (Figure 3d) lost weight with H_2 treatment. The larger weight lost for La_2O_3 was at 650 °C (0.5% in Figure 3b). Otherwise, CeO_2 increasingly lost weight at 550 °C (Figure 3d). At 750 °C it presented a 1.5% weight loss. Although the high oxygen storage capacity (OSC) of CeO_2 is well known [55], the expected weight gain of CeO_2 when treated with O_2 was not as high as the weight loss when exposed to H_2. SRE might benefit from this oxygen mobility, *i.e.*, the OSC of material can be released in the reducing environment and facilitate the SRE by oxidizing some of the carbonaceous side byproducts such as CO, as proposed in [56]. However, this oxygen vacancies are not being likely easily regenerated, which can affect the catalyst stability.

The active metals altered the reduction and oxidation capacity of all of the materials (Figure 3a–c). The reduction profile of $RhPt/La_2O_3$ (Figure 3a) showed an abrupt and significant H_2 uptake at 550 °C, 2% more than the support weight loss at the same temperature. In this case, a new crystalline phase (La hydrides, as was checked by XPS, *vide infra*) are being formed in contact with H_2 at 550 °C, which seems to be stable at higher temperatures. When this structure is formed, a lower O_2 intake capacity was observed compared with the support (Figure 3b). The formation of this new lanthana phase seems to be catalyzed by the active metals (*i.e.*, it was not formed when only the support was analyzed).

H_2 uptake was also higher on CeO_2 (Figure 3c) and ZrO_2 (Figure 3e) in the presence of the active metals; however, they both showed similar trends to those observed in the supports. For CeO_2, the metals slightly increased the O_2 uptake capacity at temperatures lower than 500 °C probably due to the easier reduction-oxidation cycle for the metals on the support. In ZrO_2, precious metals increased both H_2 and O_2 uptake within a small range.

The thermogravimetric behavior during the redox cycles were believed to be related to the active metal dispersion and reducibility of the supports. High dispersion of the active metal can make the H_2-chemisorption/reduction easier by providing more available active sites. A previous study [43] found that the presence of Pt on $CeZeO_2$ could increase the reducibility of $CeZrO_2$ by the dissociation and spillover of hydrogen from the Pt particles onto the $CeZrO_2$ surface, resulting in the formation of O vacancies and their associated Type II bridging OH groups. Meanwhile, the outstanding oxygen storage capacity (OSC) of CeO_2 [55,56], which was also indicated by its significant weight loss and rapid weight gain during the redox cycles from 500 to 800 °C in our test (Figure 3d), could improve the flexibility for the oxygen association and dissociation from the active metals, promoting their oxidation. This sample presented the higher redox capacity at 700 °C, the temperature of the stability test, which can be directly related to its better performance to decompose CH_x species after ethoxy-species adsorption (Figure 2a). However, the loss of its redox capacity can be already inferred from the activity data and oxidation-reduction cycles. These metals-support interactions before and after SRE were confirmed by the following catalyst characterization studies.

2.4.2. TEM/EDX of Reduced and Aged Catalysts

The active particle sizes of both the reduced and aged catalysts were studied by TEM to evaluate the sintering of the active phase. Figure 4 shows the TEM micrographs and particle size distributions of these materials. The mean particle sizes obtained from the TEM analysis are listed in Table 1.

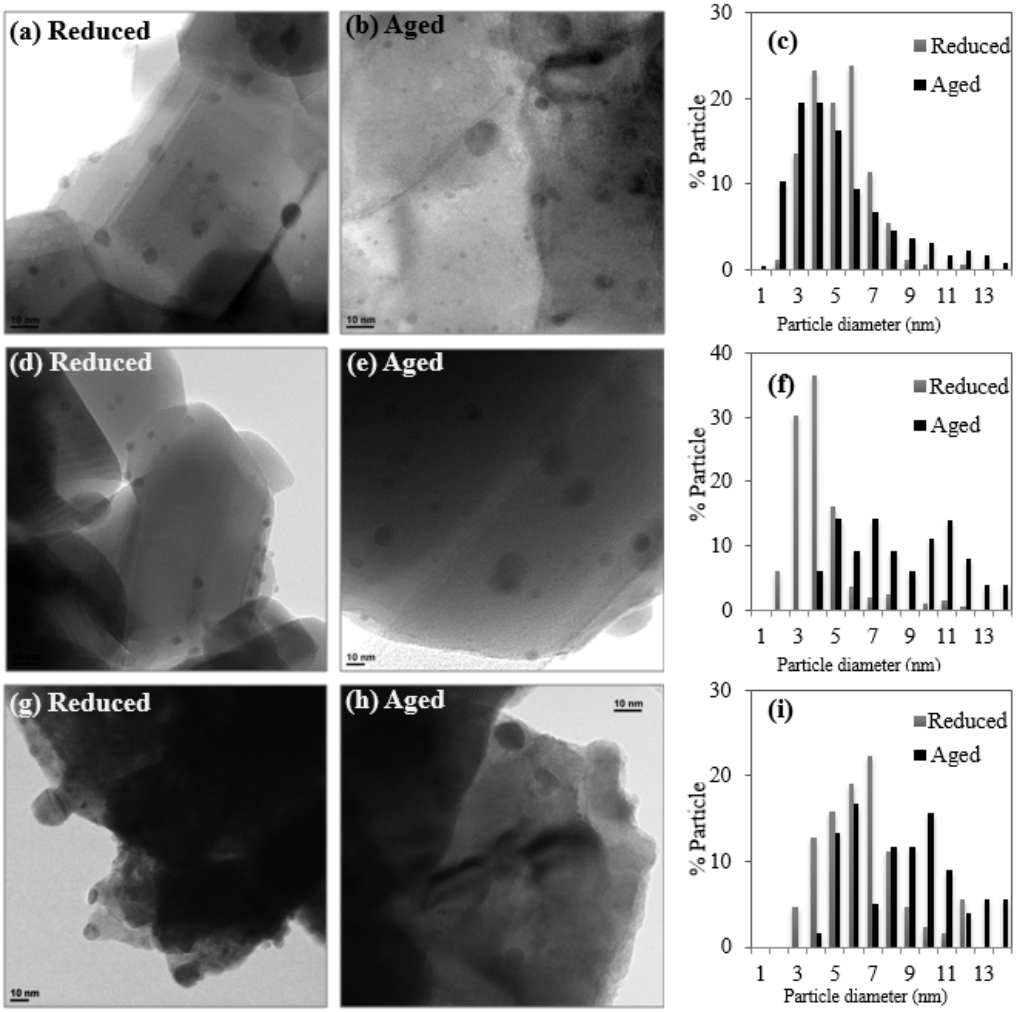

Figure 4. TEM images and particle size distribution histograms of reduced and aged catalysts: (**a**), (**b**), and (**c**) RhPt/CeO_2; (**d**), (**e**), and (**f**) RhPt/ZrO_2; (**g**), (**h**), and (**i**) RhPt/La_2O_3.

The crystalline structure of CeO_2 and the high degree of dispersion of the active sites can be observed in Figure 4a,b. The ability of CeO_2 to disperse metals on its surface is well-known [26,57,58]. The particle size of the ceria reduced catalyst suggests the presence of Rh-Pt alloys (Table 1). As was reported by Ghelamallah and Granger [51] for bimetallic Pt-Rh catalysts, the preferential formation of alloyed or bimetallic particles has been demonstrated when the particle sizes increased from ~2 nm on monometallic samples to ~5 nm on bimetallic catalysts, where the latest agrees with the particle size range obtained in this study [51]. This result is expected when the current co-impregnation method is used to prepare bimetallic catalysts [51]. The particle size distribution in RhPt/CeO_2 (Figure 4c) practically did not change during the reaction, confirming the strong metal-support interaction [22].

Similar to RhPt/CeO_2, reduced RhPt/ZrO_2 displayed a crystalline structure, small particle size, and a high degree of metal dispersion (Figure 4d). The active particle size was slightly lower in this reduced catalyst (3.6 nm, Table 1), but the particle size distribution increased in the aged sample (Figure 4e,f) and the mean particle diameter (Table 1) increased 152%. Previous reports have attributed the increase in particle size on Rh/ZrO_2 [47] and Pt/ZrO_2 [59] catalysts to the low reduction capacity of this support, as was previously found in our oxidation-reduction cycles (Section 2.4.1), which promote particle agglomeration.

In RhPt/La_2O_3 (Figure 4g–i), larger particles were observed in the reduced catalyst and the mean particle size (Table 1) increased 62%. Ghelamallah and Granger [51] evaluated Rh, Pt, and RhPt catalysts on La_2O_3 for methane reforming and reported that weak metal-support interactions promoted particle sintering under the reducing environment of the reaction. The increase in the mean particle size of the catalysts supported on ZrO_2 and La_2O_3 indicated low metal-support interaction, which allows metal particles to diffuse on the surface and promotes sintering of the active sites [58].

No important differences were detected in the ability of RhPt/CeO_2, RhPt/ZrO_2, and RhPt/La_2O_3 to convert ethanol, indicating that the augmentation of the particle size did not affect the ethanol activation step. However, the surface of small particles intrinsically contain a large amount of low-coordinated sites such as steps, kinks, and vacancies (broadly classified as defects) that have long been considered as important catalytic sites once the ethanol is activated on the catalyst surface, because the reactants and intermediaries may bind strongly to these low-coordinated sites helping breaking the chemical bonds readily. The fraction of the low-coordinated atoms increases significantly when the metal particle size decreases, ascribed to the decrease of atoms on terraces [27]. The small active particle size in RhPt/CeO_2, even in the aged sample (Figure 4b), confirms the presence of a stable active phase over this support, which better reacts to convert the adsorbed ethanol into the desirable reforming products.

In order to gain an insight in the possible particle structure, Figure 5 shows the surface chemical composition of the catalysts obtained by EDX. Rh/(Rh + Pt) ratio in reduced samples of RhPt/CeO_2 (0.58), RhPt/ZrO_2 (0.70), and RhPt/La_2O_3 (0.53) were lower than the expected (0.85), indicating a possible Pt enrichment on the catalyst surface. This enrichment could occur by a preferential interaction of Pt with H_2 during the reduction step. Gary *et al.* [18] proposed that the activation process of a Pt/CeO_2 catalyst in the SRE is favored by the H_2 presence due to Pt reacts simultaneously with H^+ species and oxygen vacancies, ensuring the availability of the active site on the catalytic surface. According to this, the reduction of the catalysts at 700 °C before reaction appears to favor the availability of Pt on the catalyst surface, mitigating its adsorption into the support. However, Rh/(Rh + Pt) ratio approached to expected in RhPt/CeO_2 and RhPt/ZrO_2 after reaction, showing a possible adsorption of Pt into either the particles or the support [60,61]. In contrast, no significant changes in Rh/(Rh + Pt) ratio of reduced and aged RhPt/La_2O_3 samples were observed, but the total content of the metals on the surface decreased. This may be related to a proportional agglomeration or adsorption of both metals (Pt and Rh) on La_2O_3 surface.

The content of Ce, Zr, and La were similar to those expected for all catalysts. The decrease in the amount of oxygen expected, which was higher in RhPt/CeO_2-R, could be attributed to the presence of oxygen vacancies on the surface [18].

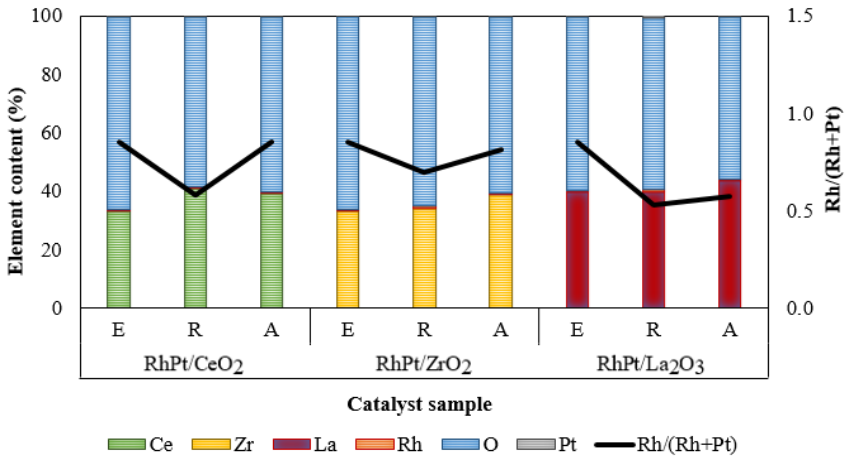

Figure 5. Energy dispersive X-ray microanalysis (EDX) of the catalyst samples by the average of three measurements over a 50 nm probe.

2.4.3. XPS

XPS can give reliable information about the oxidation state of the active metals before and after the stability test. All possible species present in the reduced and aged samples were analyzed by XPS. Table 2 lists the BEs and possible chemical structures of Rh $3d_{5/2}$, Pt $4d_{7/2}$, Ce $3d_{5/2}$, Zr $3d_{5/2}$, La $3d_{5/2}$, and Cl $2p_{3/2}$. Figure 6a shows the Rh $3d_{5/2}$ XPS spectra of the reduced and aged catalysts.

Table 2. Binding energy (BE in eV) and percent relative abundance (%, in parentheses) of the catalysts from XPS.

Element	Catalyst Sample		Possible Chemistry
	Reduced	Aged	
		$RhPt/CeO_2$	
Rh $3d_{5/2}$	309.0 (100)	ND	Rh^{+3}
Pt $4d_{7/2}$	73.1 (50)	-	Pt^{0}
	-	74.6 (100)	Pt^{+4}, Pt^{+2}
	74.9 (50)	-	Pt^{+4}
Ce $3d_{5/2}$	880.7 (4)	880.6 (4)	Ce^{+3} (Ce_2O_3)
	882.3 (22)	-	Ce^{+4} (CeO_2)
	-	882.4 (24)	Ce^{+3} (Ce_2O_3)
	884.2 (19)	884.8 (23)	Ce^{+3} (Ce_2O_3)
	888.8 (23)	888.4 (21)	Ce^{+4} (CeO_2)
	897.0 (6)	897.2 (5)	Ce^{+4} (CeO_2)
	898.3 (26)	898.5(22)	Ce^{+4} (CeO_2)
Cl $2p_{3/2}$	198.3 (100)	ND	Cl^{-}
		$RhPt/ZrO_2$	
Rh $3d_{5/2}$	307.1 (62)	307.3 (59)	Rh^{0}
	308.7 (38)	308.3 (41)	Rh^{+3}
Pt $4d_{7/2}$	71.7 (100)	71.7 (100)	Pt^{0}
Zr $3d_{5/2}$	182.0 (100)	182.0 (100)	Zr^{+4} (ZrO_2)
Cl $2p_{3/2}$	ND	ND	-

Table 2. *Cont.*

Element	Catalyst Sample		Possible Chemistry
	Reduced	Aged	
		$RhPt/La_2O_3$	
Rh $3d_{5/2}$	-	307.2 (58)	Rh^0
	308.9 (82)	308.9 (42)	Rh^{+3}
	310.1 (18)	-	Rh^{+3} ($RhCl_3$)
Pt $4d_{7/2}$	ND	ND	ND
La $3d_{5/2}$	834.9 (54)	834.8 (54)	La^{+3} (La_2O_3)
	837.3 (15)	837.3 (14)	La^{+3} (LaH_2^{+1})
	838.7 (31)	838.7 (32)	La^{+3} (LaH_3)
Cl $2p_{3/2}$	195.5 (71)	195.5 (73)	Metal-Cl
	198.3(29)	198.2 (27)	Cl^-

ND: Not detected

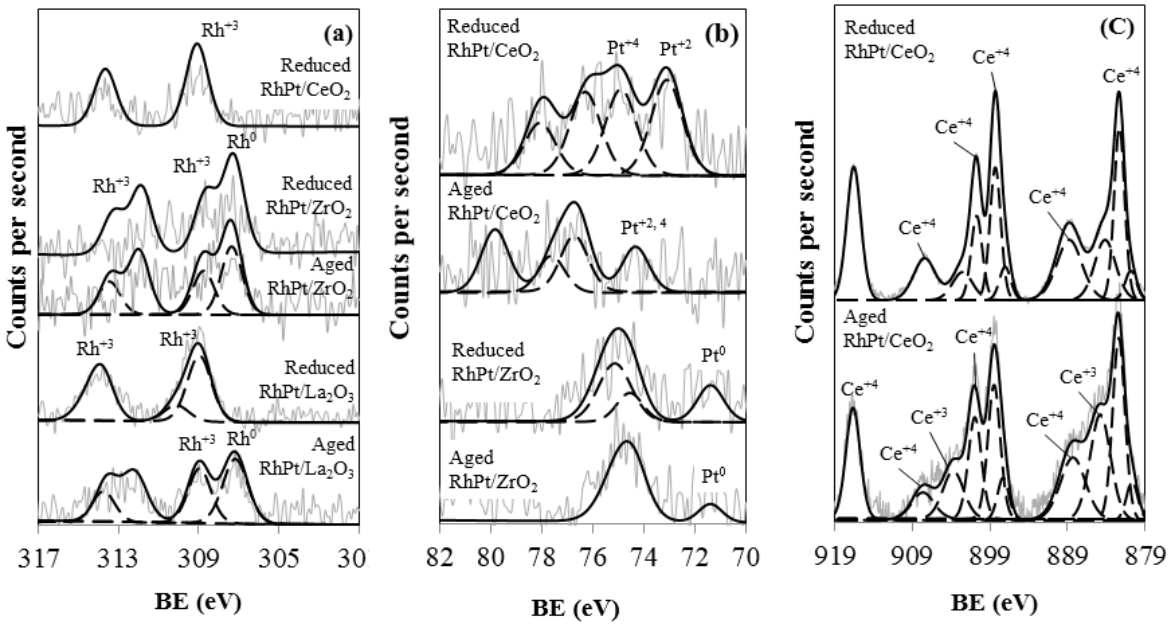

Figure 6. XPS spectra of (**a**) Rh $3d_{5/2}$; (**b**) Pt $7f_{7/2}$; and (**c**) Ce $3d_{3/2}$ and $3d_{5/2}$ for reduced and aged catalysts.

In general, two main oxidation states were observed in Rh $3d_{5/2}$: Rh^{+3} (308.3–310.5 eV) and Rh^0 (307.0–307.7 eV).[58,62] In reduced $RhPt/CeO_2$, only Rh^{+3} was identified, which is associated with rhodium oxides and small amounts of metal precursor, confirmed by the presence of Cl in the sample [58]. Avgouropoulos *et al.* [63] reported the presence of exclusively Rh^{+3} after reduction at 300 °C over CeO_2 owing to oxygen transfer to the metal from the support. On the other hand, Rh was not detected in aged $RhPt/CeO_2$. This could be ascribed to the fact that the CeO_2 crystal size may interfere with the quantification of Rh particles on the surface [64] and a consequence of the Pt surface enrichment found by EDX (see Section 2.4.2).

In reduced $RhPt/CeO_2$, Pt^{+4} (74.9 eV, 50%) and Pt^0 (73.1 eV, 50%) were identified (Figure 6b). Aged $RhPt/CeO_2$ showed only one peak attributed to both Pt^{+4} and Pt^{+2}, informing about a complete Pt

oxidation during the stability test [65]. As reported by Kaila *et al.* [61], the presence of an alloy on these bimetallic catalysts is possible with all Rh/Pt ratios because of the miscibility of the Rh_xPt_{1-x} system. The Rh_xPt_{1-x} alloys result in a strong Pt enrichment of the surface as the temperature increases [35,47] which agrees with our results on the aged $RhPt/CeO_2$ catalyst, where Rh was not observed on the surface by XPS and diminished its surface concentration in EDX (Section 2.4.2). The strong oxidation state of the metals on this catalyst is consistent to the great oxygen mobility from the CeO_2 support. In the case of SRE, one point of common agreement is that the oxygen mobility of the support is a critical property to favor C removal and avoid deactivation [27].

Figure 6c shows the Ce $3d_{3/2}$ and $3d_{5/2}$ XPS spectra of both reduced and aged $RhPt/CeO_2$. Although the determination of the cerium oxide state from Ce 3d level spectra is difficult, we reviewed several publications trying to establish the contribution of Ce^{+3} and Ce^{+4} in each catalyst sample. Ce^{+4} could be ascribed to shoulders at 882, 888, 899, 901, 908, and 917 eV, [55,60,66] and Ce^{+3} can be seen at 885 and 903 eV [55,60,64]. Both species play an important role in the catalytic process. Ce^{+4} acts as a Lewis acid by interacting with the O (2p) orbital of alcohols to form hydroxyl species that are intermediates in ethanol decomposition [60,61]. The presence of Ce^{+3} indicates the reduction of the CeO_2 surface by interactions between a noble metal and Ce [67]. Rh and Pt have been proposed to occupy the oxygen vacancies in the CeO_2 lattice, promoting Ce^{+3} formation [60] and preventing metal movement on the oxide surface [55], as confirmed by TEM (Section 2.4.2).

The selected characteristic Ce^{+3} shoulder (885.5 and 903 eV) [64] increased by 126% in the aged sample, while the amount of Ce^{+4} decreased by 38% (Figure 6c). This established that the Ce^{+3}/Ce^{+4} ratio increased in the ceria supported catalyst from 0.3 (reduced) to 1.1 (aged). These results agree with oxidation/reduction cycles (Section 2.4.1) and may result from a change in the distribution of oxygen vacancies on the catalytic surface promoted by reducing agents present in the reaction system [68]. Divins *et al.* [46] evaluated a $RhPd/CeO_2$ catalyst in the SRE, also reporting an increase in the Ce^{+3}/Ce^{+4} ratio from 0.63 to 0.83 after reaction at 550 °C. The authors suggested that the capability of CeO_2 as a support to activate water and to donate oxygen atoms could oxidize noble metals in the SRE. The increase in Ce^{+3} facilitates metal particle dispersion on the catalyst surface, but the loss of Ce^{+4} may cause the observed reduction of CH_4 reforming capacity for $RhPt/CeO_2$ with TOS (Figure 2b). Higher oxygen storage capacity and oxygen mobility allow a more effective gasification/oxidation of adsorbed carbon on the catalyst. Furthermore, the high oxygen mobility could facilitate the oxygen migration to the metal-support interface, which would favor the oxidation of $*CH_x$ species [27]. But it seems that Ce^{+4} is not regenerated during the reaction not only because of the lack of an oxygen source in the reaction media, but also by its difficulty of gaining oxygen in redox cycles (Section 2.4.1). Water adsorption can also help to the ceria re-oxidation [27], but the low S/E ratio of three used in the current experiments limits the oxygen source.

On the contrary, most Rh in reduced $RhPt/ZrO_2$ was Rh^0 (62%, Table 2), consistent with the results of Tanabe *et al.* [69], who proposed that the low interaction between ZrO_2 and Rh favors metal reduction and promotes sintering, as observed here (Figure 4). The Rh^{+3} species, associated with Rh_2O_3, was also present. The oxidation state of the Rh species was stable after aging. Only Pt^0 (71.7 eV) was detected in reduced and aged $RhPt/ZrO_2$. The stability of reduced Pt was previously reported for a Pt/ZrO_2 catalyst [61,67]. This metal accommodation over the support seems to affect H_2 selectivity, as observed in Figure 1b. The reduced metallic species seems to have less degree of interaction with the support,

promoting agglomeration (9.1 nm, Table 1) and affecting reactant-catalyst interphase. The characteristic peak for Zr $3d_{5/2}$ (182 eV) has been ascribed to Zr^{+4} in the zirconia support (Table 2) [26]. There was no appreciable difference in the zirconium oxide structure between the reduced and aged catalysts.

The Rh $3d_{5/2}$ spectra had two peaks in the reduced RhPt/La_2O_3 catalyst sample (Table 2, Figure 6a), one at 310.1 eV corresponding to an oxidized Rh^{3+} species linked to the metal precursor (confirmed by the Cl 2p spectra) and another at 308.9 eV, which indicates the presence of Rh_2O_3 [30]. After aging, the latter signal decreased and Rh^0 appeared. However, Pt was not detected on the RhPt/La_2O_3 samples; hence, it was not possible to confirm the surface Pt enrichment observed on RhPt/CeO_2 and reported by Ghelamallah and Granger on RhPt/La_2O_3 [51]. The particle agglomeration observed by TEM and the encapsulation into the support suggested by EDX might be related to this obstruction. Moreover, the presence of metallic particles on zirconia and lanthana supported catalysts seems to be directly related to the metal agglomeration. The La $3d_{5/2}$ XPS peaks at 834, 837, and 838 eV were ascribed to La_2O_3, LaH_2^{+1}, and LaH_3, respectively [51,70]. These species remained almost constant after aging (Table 2) and confirmed the presence of La hydrides on the support, which was observed in oxidation/reduction cycles (see Section 2.4.1).

2.4.4. TGA

Coke formation can be evaluated by TGA in air. Table 1 shows the TGA results for reduced and aged catalysts. No significant differences were observed between both samples at ceria and zirconia catalysts, consistent with their basic nature [59,71,72]. The RhPt/La_2O_3 behavior is ascribed to the La hydrides reaction with oxygen, which is favored in the presence of active metals, as was found in the oxidation/reduction cycles of this support (Section 2.4.1) [30,73]. However, no important differences were recorded between reduced and aged samples, showing that this La hydrides decomposition on the support is the main weight loss cause. In general, results indicate that carbonaceous residues did not play an important role in determining the stability of the catalysts, confirming that basic supports may reduce the formation of carbonaceous compounds [13,36,64,72].

As mentioned by Zanchet *et al.* [27] the control of carbon accumulation depends on the availability of surface oxygen required to oxidize the *C species. Contrarily to base metals, carbon nucleation is energetically unfavorable in noble metal surfaces, reducing the solubility of carbon on the later materials. Nobel metal lattice is too large compared to graphene lattice, hindering its formation. They suggested that the geometric effect is more important than the electronic one. Hence, only superficial carbon is usually formed on supported noble metal catalysts.

From these results, changes in the selectivity of RhPt/La_2O_3 and RhPt/ZrO_2 with TOS can be related to metal sintering caused by active phase characteristics. In addition, both catalysts presented more stable reduced Rh and Pt species than the CeO_2 counterpart did, which can indicate that the lack of oxidized metals promotes their sintering on the support, because a low metal-support interaction [69]. This changes hydrogenation/dehydrogenation mechanisms that are structure-sensitivity and affect the oxygen mobility throughout the catalyst, necessary to finally oxidize the CH_x species previously activated on the catalytic surface. However, it is important to remark that both catalysts presented showed constant complete ethanol conversion during the stability test, stable H_2 selectivity, and the absence of carbon deposition. Moreover, RhPt/CeO_2 showed that the metals can be forming small and

stable Rh-Pt alloys containing both Rh and Pt oxidized species from the beginning of the reaction, which make this catalyst more selective to H_2. This catalyst show a greater oxygen mobility, which seems to travel from the support, crossing the active metals, and reaching the CH_x species to finally oxidize them, producing H_2, CO, and CO_2. These features could be exploited in the reforming of raw bioethanol samples. Divins *et al.* [74] reported similar product distribution when reforming synthetic ethanol/water and raw bioethanol samples over a $RhPd/CeO_2$ catalyst, due to a synergy between the active metals and the support. However, the changing Ce^{+3}/Ce^{+4} ratio during the stability test can slightly affect the catalyst selectivity during larger period of times. Therefore, longer stability tests and different catalyst reactivation methods will be evaluated in our laboratory using the $RhPt/CeO_2$ catalyst. It is important to remark that a delicate equilibrium between Ce^{+3}/Ce^{+4} ratio must be assured to provide for catalyst stability. In addition, we are currently studying the effect of the Rh/Pt ratio on ceria on the product and byproduct distribution.

3. Experimental Section

3.1. Catalyst Synthesis

The catalysts were prepared by the incipient wetness co-impregnation method. The active metals were obtained from rhodium (III) chloride hydrate ($RhCl_3 \cdot H_2O$) (Sigma-Aldrich, St. Louis, MO, USA) and chloroplatinic acid hexahydrate ($H_2PtCl_6 \cdot 6H_2O$) (Sigma-Aldrich) solutions in water. The CeO_2, ZrO_2, and La_2O_3 supports were obtained from the calcination of cerium nitrate hexahydrate (99.5%, Alfa Aesar, Haverhill, MA, USA), zirconium (IV) oxide (99.9%, Alfa Aesar), and lanthanum (III) oxide (98%, Panreac, Castellar del Valles, Barcelona, Spain), respectively, at 700 °C in a muffle oven for 2 h. Metals loading of 0.6 wt. % Rh and 0.2 wt. % Pt were selected, based in previous investigations in which this ratio was found to be the more active for reforming reactions [30,61]. Low amounts of active metals (0.8 wt. % total) were employed to contribute to the economy of the process. The required amounts of active metals were co-impregnated onto the supports. To achieve co-impregnation, the metal-support mixture was continuously stirred, dried at 100 °C for 24 h, and calcined at 700 °C in air for 2 h. All the calcined solids were sieved using an 80 mesh sieve to ensure particle sizes of less than 177 μm. These samples are the "fresh (F)" catalysts.

3.2. Catalytic Tests

The catalytic performance of $RhPt/CeO_2$, $RhPt/ZrO_2$, and $RhPt/La_2O_3$ was evaluated in a fixed bed reactor at atmospheric pressure under kinetic control. The catalyst particles (100 mg) were diluted by mixing with quartz particles (200 mg, 80-mesh). The catalyst mixture was loaded into a quartz tube reactor (12 mm ID) with a frit fused equidistant from both ends of the tube. The plug flow reactor condition was achieved by eliminating back mixing and channeling when a ratio of 45 was maintained between the catalyst bed height and catalyst particle size (L/Dp) and a ratio of 60 was maintained between the reactor internal diameter and catalyst particle size (D/Dp) [75,76]. Before the reaction, the catalysts were reduced in 10% H_2/N_2 (300 mL/min) at 700 °C for 1 h (these samples are the "reduced (R)" catalysts). Then, a premixed solution of ethanol (99.9%, ACS grade, J.T. Baker, Center Valley, PA, USA) and distilled water was pumped continuously into the heated reaction system with a Simdos

02 metering pump (KNF Neuberger, Trenton, NJ, USA). The vaporized reactants combined with the incoming N_2 (diluent and internal standard) and passed through the catalyst bed. For each test, the EtOH:H_2O:N_2 molar ratio was adjusted to 1:3:51 (stoichiometric S/E molar ratio), in order to avoid mass transfer limitations in the system [39], and the total gas flow was 300 mL/min.

Each catalytic activity test was conducted at GHSV of 70,600 h^{-1} at atmospheric pressure between 400 and 700 °C in 20 °C increments (continuous sequence, 25 min at each temperature). Blank tests were performed using an empty reactor or only the support, previously reduced, under the same conditions. In addition, 27 h time on stream (TOS) SRE catalytic stability tests were conducted at 700 °C for each reduced catalyst using the conditions and parameters described above. The samples used in these stability tests are the "aged (A)" catalysts. Following these tests, the aged catalysts were subjected to an activity test between 400 and 700 °C to evaluate possible activity loss.

The compounds in the product stream, including H_2, CH_4, CO, CO_2, ethanol, and ethylene, were quantified online using a Clarus 580 gas chromatograph (GC, Perkin Elmer, Norwalk, CT, USA) equipped with a Carboxen 1010 plot column (30 m, 0.53 mm ID, Restek, Bellefonte, PA, USA) connected to a thermal conductivity detector (TCD) and an Innowax column (30 m, 0.53 mm ID, Perkin Elmer, Boston, MA, USA) connected to a flame ionization detector (FID). Elemental balances between the inlet ethanol-water feed and the outlet products were measured in all tests. The test was declared effective when the elemental carbon balance was ~100%.

The ethanol conversion (X_{EtOH}), yield, and mole distribution for each detected product were calculated according to Equations (15)–(17):

$$X_{EtOH} = \frac{F_{\mathrm{EtOH,o}} - F_{\mathrm{EtOH,t}}}{F_{\mathrm{EtOH,o}}} \quad (15)$$

$$Yield_i = \frac{\text{Mole of } i}{\text{Mole of etanol inlet}} \quad (16)$$

$$Mole\ fraction_i = \frac{F_i}{\sum F_i} \times 100\% \quad (17)$$

where $F_{EtOH,o}$ is the initial theoretical mole flow (mol/min) of ethanol at ambient temperature, $F_{EtOH,t}$ is the mole flow (mol/min) of unreacted ethanol in the product stream detected by GC at time t, and F_i is the mole flow (mol/min) of product i (H_2, CO, CH_4, CO_2, or C_2H_4). Thermodynamic equilibrium calculations were simulated using Aspen Hysys 7.3 software (2011, Burlington, MA, USA) by taking into account all the possible reactions (Equations (2)–(10)) [5–7].

3.3. Catalyst Characterization

Fresh catalysts were characterized by oxidation-reduction cycle analysis with a TG/DSC unit (Netzsch® Jupiter STA 449 F3, Selb/Bavaria, Germany) to evaluate the sample reducibility. 10 mg of fresh sample was placed in an alumina crucible and 1% O_2/N_2, 4% H_2/N_2, in pure N_2 as diluent were used. The sample was initially heated to 150 °C in pure N_2. After steady state at 150 °C was reached, oxidizing and reducing gases were alternately introduced. In between reduction and oxidation, pure N_2 was introduced to purge the remaining reactive gas. TG/DSC signals were recorded simultaneously. Each oxidation/reduction cycle was carried out isothermally at temperatures ranging from 150–750 °C. The temperature interval was set to be 100 °C. The sample was heated after the completion of each cycle

with 1 °C/min in N_2 to the next temperature stage. The extent of sample reduction and re-oxidation was quantified by Equations (18) and (19).

$$\Delta W_{O_2}^{T_{iso}} = W_{O_2}^{T_{iso,end}} - W_{O_2}^{T_{iso,start}} \quad (18)$$

$$\Delta W_{H_2}^{T_{iso}} = W_{H_2}^{T_{iso,end}} - W_{H_2}^{T_{iso,start}} \quad (19)$$

where $\Delta W_{O_2}^{T_{iso}}$ or $\Delta W_{H_2}^{T_{iso}}$ is the sample weight change (%) during the isothermal oxidation or reduction process at programmed temperature T_{iso} .

The TEM experiments were conducted to reduced and aged catalyst samples using a JEOL JEM-2010 microscope at 200 kV coupled to energy-dispersive X-ray spectroscopy (EDX, INCA Energy TEM100, Oxford Instruments, Abingdon, Oxfordshire, UK) with a Si(Li) detector, 30 mm^2 detection area, and 142 eV resolution. The samples were dispersed in ethanol by ultrasonic vibration and dropped on a carbon film-coated copper grid. The active metal particles were measured with ImageJ software, counting at least 100 particles per image. The mean particle diameter was calculated according to Equation (20), where n_i is the number of particles and d_i is the particle diameter [77,78], and particle size distribution histograms were constructed [79].

$$\bar{d}_p = \sum_i n_i d_i^3 \Big/ \sum_i n_i d_i^2 \quad (20)$$

XPS spectra of reduced and aged catalysts were obtained using an electron spectrometer (VG-Microtech Multilab, East Grinstead, West Sussex, UK) with a twin anode radiation source in the Mg Kα (1253.6 eV) constant energy analysis mode and an energy flow of 50 eV. The analysis chamber was maintained at 5.10×10^{-8} Pa. The C 1s line was set at 248.6 eV. The binding energy (BE) values were obtained with a precision of 0.2 eV using the Peak Fit program of the spectrometer control program.

The TGA/DTG analysis for reduced and aged samples was performed in a thermogravimetric analyzer (Mettler Toledo, Columbus, OH, USA). Each sample (30 mg) was pretreated in pure N_2 at 100 °C and subsequently heated to 1000 °C in air (5 °C/min, 100 mL/min flow rate) to burn off the deposits.

4. Conclusions

Steam reforming of ethanol for hydrogen production was evaluated on RhPt bimetallic catalysts supported on CeO_2, ZrO_2, and La_2O_3 with 0.6 wt. % Rh and 0.2 wt. % Pt loading. RhPt/CeO_2 showed the highest hydrogen production in the catalytic activity tests, followed by RhPt/La_2O_3 and RhPt/ZrO_2. RhPt/CeO_2 was found to be the most selective catalyst, possibly owing to the strong interactions between the metal particles and catalyst support, which resulted in metal particles smaller than 5 nm on the support that probably consisted of Rh-Pt alloys with a Pt surface enrichment. There, both metals were completely oxidized. The considerable oxygen storage capacity of the CeO_2 support was confirmed by the presence of Ce^{+3}/Ce^{+4}. However, the reduction of Ce^{+4} species, which are considered the active sites where reactants and intermediates interact, could be responsible for the loss of methane reforming on RhPt/CeO_2 during the stability test, affecting H_2 production and byproduct distribution.

Although ZrO_2 and La_2O_3 supported catalysts performed well in the stability test, the active metals (Rh and Pt) underwent rapid sintering on these supports, resulting in their lower H_2 selectivity compared

with $RhPt/CeO_2$. The metal sintering of both catalysts seems to be related to the limited oxidation of the active phase, which in turn affects the hydrogenation/dehydrogenation reactions to convert the adsorbed ethoxy-species into reforming products.

Nevertheless, the three supported catalysts were not affected by carbonaceous residues under the current SRE conditions, probably because of the noble metals presence and the support basic nature, which avoids undesirable coking of reaction intermediates.

Acknowledgments

The authors are grateful to the Universidad de La Sabana and Universidad de Alicante for the financial support of this work. Martha Cobo acknowledges Robert Farrauto (Columbia University) for his insights on the development of this work.

Author Contributions

This work was developed in equal parts by Martha Cobo and Bernay Cifuentes. Juan A. Conesa participated in the characterization of catalysts through performing techniques such as TEM, EDX, and XPS. Manuel F. Valero advised TGA analyzes and reaction system assembly. However, all the authors contributed to the writing and review of this document.

Conflicts of Interest

The authors declare no conflict of interest.

References

1. Yu, C.Y.; Lee, D.W.; Park, S.J.; Lee, K.Y.; Lee, K.H. Study on a catalytic membrane reactor for hydrogen production from ethanol steam reforming. *Int. J. Hydrogen Energy* **2009**, *34*, 2947–2954.
2. Vizcaíno, A.J.; Lindo, M.; Carrero, A.; Calles, J.A. Hydrogen production by steam reforming of ethanol using Ni catalysts based on ternary mixed oxides prepared by coprecipitation. *Int. J. Hydrogen Energy* **2012**, *37*, 1985–1992.
3. Wang, Z.; Wang, C.; Chen, S.; Liu, Y. Co-Ni bimetal catalyst supported on perovskite-type oxide for steam reforming of ethanol to produce hydrogen. *Int. J. Hydrogen Energy* **2014**, *39*, 5644–5652.
4. Guerrero, L.; Castilla, S.; Cobo, M. Advances in ethanol reforming for the production of hydrogen. *Quim. Nova* **2014**, *37*, 850–856.
5. Liberatori, J.W.C.; Ribeiro, R.U.; Zanchet, D.; Noronha, F.B.; Bueno, J.M.C. Steam reforming of ethanol on supported nickel catalysts. *Appl. Catal. A* **2007**, *327*, 197–204.
6. Valle, B.; Aramburu, B.; Remiro, A.; Bilbao, J.; Gayubo, A.G. Effect of calcination/reduction conditions of Ni/La_2O_3-αAl_2O_3 catalyst on its activity and stability for hydrogen production by steam reforming of raw bio-oil/ethanol. *Appl. Catal. B* **2014**, *147*, 402–410.
7. Wang, H.; Zhang, L.; Yuan, M.; Xu,T.; Liu, Y. Steam reforming of ethanol over $Ni/Ce_{0.7}Pr_{0.3}O_2$ catalyst. *J. Rare Earths* **2012**, *30*, 670–675.
8. Bilala, M. Jackson, S.D.; Bilal, M.; Jackson, S.D. Ethanol steam reforming over Rh and Pt catalysts: Effect of temperature and catalyst deactivation. *Catal. Sci. Technol.* **2013**, *3*, 754–766.

9. Zhang, C.; Yue, H.; Huang, Z.; Li, S.; Wu, G.; Ma, X.; Gong, J. Hydrogen Production via Steam Reforming of Ethanol on Phyllosilicate-Derived Ni/SiO_2: Enhanced Metal-Support Interaction and Catalytic Stability. *ACS Sustain. Chem. Eng.* **2012**, *1*, 161–173.
10. Mathure, P.V.; Ganguly, S.; Patwardhan, A.V.; Saha, R.K. Steam Reforming of Ethanol Using a Commercial Nickel-Based Catalyst. *Ind. Eng. Chem. Res.* **2007**, *46*, 8471–8479.
11. Laosiripojana, N.; Assabumrungrat, S.; Charojrochkul, S. Steam reforming of ethanol with co-fed oxygen and hydrogen over Ni on high surface area ceria support. *Appl. Catal. A* **2007**, *327*, 180–188.
12. Barattini, L.; Ramis, G.; Resini, C.; Busca, G.; Sisani, M.; Costantino, U. Reaction path of ethanol and acetic acid steam reforming over Ni–Zn–Al catalysts. Flow reactor studies. *Chem. Eng. J.* **2009**, *153*, 43–49.
13. Seker, E. The catalytic reforming of bio-ethanol over SiO_2 supported ZnO catalysts: The role of ZnO loading and the steam reforming of acetaldehyde. *Int. J. Hydrogen Energy* **2008**, *33*, 2044–2052.
14. Domínguez, M.; Taboada, E.; Molins, E.; Llorca, J. Co-Fe-Si Aerogel Catalytic Honeycombs for Low Temperature Ethanol Steam Reforming. *Catalysts* **2012**, *2*, 386–399.
15. De Souza, G.; Ávila, V.C.; Marcílio, N.R.; Perez-Lopez, O.W. Synthesis Gas Production by Steam Reforming of Ethanol over M-Ni-Al Hydrotalcite-type Catalysts; M = Mg, Zn, Mo, Co. *Procedia Eng.* **2012**, *42*, 1805–1815.
16. Wei, J.; Qian, Y.; Liu, W.; Wang, L.; Ge, Y.; Zhang, J.; Yu, J.; Ma, X. Effects of particle composition and environmental parameters on catalytic hydrodechlorination of trichloroethylene by nanoscale bimetallic Ni-Fe. *J. Environ. Sci.* **2014**, *26*, 1162–1170.
17. Song, H.; Zhang, L.; Ozkan, U.S. Investigation of the Reaction Network in Ethanol Steam Reforming over Supported Cobalt Catalysts. *Ind. Eng. Chem. Res.* **2010**, *49*, 8984–8989.
18. Jacobs, G.; Keogh, R.A.; Davis, B.H. Steam reforming of ethanol over Pt/ceria with co-fed hydrogen. *J. Catal.* **2007**, *245*, 326–337.
19. Idriss, H.; Scott, M.; Llorca, J.; Chan, S.C.; Chiu, W.; Sheng, P.-Y.; Yee, A.; Blackford, M.A.; Pas, S.J.; Hill, A.J.; *et al*. A phenomenological study of the metal-oxide interface: The role of catalysis in hydrogen production from renewable resources. *ChemSusChem* **2008**, *1*, 905–910.
20. Costa, L.O.O.; Vasconcelos, S.M.R.; Pinto, A.L.; Silva, A.M.; Mattos, L.V.; Noronha, F.B.; Borges, L.E.P. Rh/CeO_2 catalyst preparation and characterization for hydrogen production from ethanol partial oxidation. *J. Mater. Sci.* **2007**, *43*, 440–449.
21. Coronel, L.; Múnera, J.F.; Tarditi, A.M.; Moreno, M.S.; Cornaglia, L.M. Hydrogen production by ethanol steam reforming over Rh nanoparticles supported on lanthana/silica systems. *Appl. Catal. B* **2014**, *160–161*, 254–266.
22. Hou, T.; Yu, B.; Zhang, S.; Xu, T.; Wang, D.; Cai, W. Hydrogen production from ethanol steam reforming over Rh/CeO_2 catalyst. *Catal. Commun.* **2015**, *58*, 137–140.
23. Lin, W.-H.; Liu, Y.-C.; Chang, H.-F. Hydrogen production from oxidative steam reforming of ethanol in a palladium-silver alloy composite membrane reactor. *J. Chin. Inst. Chem. Eng.* **2008**, *39*, 435–440.
24. Vaidya, P.D.; Rodrigues, A.E. Kinetics of Steam Reforming of Ethanol over a Ru/Al_2O_3 Catalyst. *Ind. Eng. Chem. Res.* **2006**, *45*, 6614–6618.

25. Hou, T.; Zhang, S.; Xu, T.; Cai, W. Hydrogen production from oxidative steam reforming of ethanol over Ir/CeO_2 catalysts in a micro-channel reactor. *Chem. Eng. J.* **2014**, *255*, 149–155.
26. Idriss, H. Ethanol Reactions over the Surfaces of Noble Metal/Cerium Oxide Catalysts. *Platin. Met. Rev.* **2004**, *48*, 105–115.
27. Zanchet, D.; Santos, J.B.O.; Damyanova, S.; Gallo, J.M.R.; Bueno, J.M.C. Toward Understanding Metal-Catalyzed Ethanol Reforming. *ACS Catal.* **2015**, *5*, 3841–3863.
28. Le Valant, A.; Can, F.; Bion, N.; Duprez, D.; Epron, F. Hydrogen production from raw bioethanol steam reforming: Optimization of catalyst composition with improved stability against various impurities. *Int. J. Hydrogen Energy* **2010**, *35*, 5015–5020.
29. Da Silva, A.M.; de Souza, K.R.; Jacobs, G.; Graham, U.M.; Davis, B.H.; Mattos, L.V.; Noronha, F.B. Steam and CO_2 reforming of ethanol over Rh/CeO_2 catalyst. *Appl. Catal. B* **2011**, *102*, 94–109.
30. Cobo, M.; Pieruccini, D.; Abello, R.; Ariza, L.; Córdoba, L.F.; Conesa, J.A. Steam reforming of ethanol over bimetallic RhPt/La_2O_3: Long-term stability under favorable reaction conditions. *Int. J. Hydrogen Energy* **2013**, *38*, 5580–5593.
31. Contreras, J.L.; Salmones, J.; Colín-Luna, J.A.; Nuño, L.; Quintana, B.; Córdova, I.; Zeifert, B.; Tapia, C.; Fuentes, G.A. Catalysts for H_2 production using the ethanol steam reforming (a review). *Int. J. Hydrogen Energy* **2014**, *39*, 18835–18853.
32. Karatzas, X.; Jansson, K.; González, A.; Dawody, J.; Pettersson, L.J. Autothermal reforming of low-sulfur diesel over bimetallic RhPt supported on Al_2O_3, CeO_2-ZrO_2, SiO_2 and TiO_2. *Appl. Catal. B* **2011**, *106*, 476–487.
33. Barroso, M.N.; Gomez, M.F.; Arrúa, L.A.; Abello, M.C. Co catalysts modified by rare earths (La, Ce or Pr) for hydrogen production from ethanol. *Int. J. Hydrogen Energy* **2014**, *39*, 8712–8719.
34. Maia, T.A.; Assaf, J.M.; Assaf, E.M. Study of Co/CeO_2-γ-Al_2O catalysts for steam and oxidative reforming of ethanol for hydrogen production. *Fuel Process. Technol.* **2014**, *128*, 134–145.
35. De Lima, S.M.; Silva, A.M.; Graham, U.M.; Jacobs, G.; Davis, B.H.; Mattos, L.V.; Noronha, F.B. Ethanol decomposition and steam reforming of ethanol over $CeZrO_2$ and Pt/$CeZrO_2$ catalyst: Reaction mechanism and deactivation. *Appl. Catal. A* **2009**, *352*, 95–113.
36. Arslan, A.; Gunduz, S.; Dogu, T. Steam reforming of ethanol with zirconia incorporated mesoporous silicate supported catalysts. *Int. J. Hydrogen Energy* **2014**, *39*, 18264–18272.
37. Hou, T.; Zhang, S.; Chen, Y.; Wang, D.; Cai, W. Hydrogen production from ethanol reforming: Catalysts and reaction mechanism. *Renew. Sustain. Energy Rev.* **2015**, *44*, 132–148.
38. López, E.; Divins, N.J.; Llorca, J. Hydrogen production from ethanol over Pd–Rh/CeO_2 with a metallic membrane reactor. *Catal. Today* **2012**, *193*, 145–150.
39. Heck, R.M.; Farrauto, R.J.; Gulati, S.T. *Catalytic Air Pollution Control: Commercial Technology*; John Wiley & Sons: Hoboken, NJ, USA, 2009.
40. Peela, N.R.; Kunzru, D. Oxidative steam reforming of ethanol over Rh based catalysts in a micro-channel reactor. *Int. J. Hydrogen Energy* **2011**, *36*, 3384–3396.
41. Rossetti, I.; Biffi, C.; Bianchi, C.L.; Nichele, V.; Signoretto, M.; Menegazzo, F.; Finocchio, E.; Ramis, G.; di Michele, A. Ni/SiO_2 and Ni/ZrO_2 catalysts for the steam reforming of ethanol. *Appl. Catal. B* **2012**, *117–118*, 384–396.
42. Zou, J.; Yu, B.; Zhang, S.; Zhang, J.; Chen, Y.; Cui, L.; Xu, T.; Cai, W. Hydrogen production from ethanol over Ir/CeO_2 catalyst: Effect of the calcination temperature. *Fuel* **2015**, *159*, 741–750.

43. De Lima, S.M.; Silva, A.M.; da Cruz, I.O.; Jacobs, G.; Davis, B.H.; Mattos, L.V.; Noronha, F.B. H_2 production through steam reforming of ethanol over Pt/ZrO_2, Pt/CeO_2 and Pt/$CeZrO_2$ catalysts. *Catal. Today* **2008**, *138*, 162–168.
44. Da Silva, A.M.; Mattos, L.V.; Múnera, J.; Lombardo, E.; Noronha, F.B.; Cornaglia, L. Study of the performance of Rh/La_2O_3-SiO_2 and Rh/CeO_2 catalysts for SR of ethanol in a conventional fixed-bed reactor and a membrane reactor. *Int. J. Hydrogen Energy* **2015**, *40*, 4154–4166.
45. Graschinsky, C.; Lupiano Contreras, J.; Amadeo, N.; Laborde, M. Ethanol Oxidative Steam Reforming over Rh(1%)/$MgAl_2O_4$/Al_2O_3 Catalyst. *Ind. Eng. Chem. Res.* **2014**, *53*, 15348–15356.
46. Divins, N.J.; Angurell, I.; Escudero, C.; Pérez-Dieste, V.; Llorca, J. Influence of the support on surface rearrangements of bimetallic nanoparticles in real catalysts. *Science* **2014**, *346*, 620–623.
47. Scarabello, A.; Dalle Nogare, D.; Canu, P.; Lanza, R. Partial oxidation of methane on Rh/ZrO_2 and Rh/Ce-ZrO_2 on monoliths: Catalyst restructuring at reaction conditions. *Appl. Catal. B* **2015**, *174–175*, 308–322.
48. Vargas, J.C.; Ivanova, S.; Thomas, S.; Roger, A.-C.; Pitchon, V. Influence of Gold on Ce-Zr-Co Fluorite-Type Mixed Oxide Catalysts for Ethanol Steam Reforming. *Catalysts* **2012**, *2*, 121–138.
49. Martono, E.; Vohs, J.M. Support effects in cobalt-based ethanol steam reforming catalysts: Reaction of ethanol on Co/CeO_2/YSZ(100) model catalysts. *J. Catal.* **2012**, *291*, 79–86.
50. Munera, J.; Irusta, S.; Cornaglia, L.; Lombardo, E.; Vargascesar, D.; Schmal, M. Kinetics and reaction pathway of the CO_2 reforming of methane on Rh supported on lanthanum-based solid. *J. Catal.* **2007**, *245*, 25–34.
51. Ghelamallah, M.; Granger, P. Supported-induced effect on the catalytic properties of Rh and Pt-Rh particles deposited on La_2O_3 and mixed α-Al_2O_3-La_2O_3 in the dry reforming of methane. *Appl. Catal. A* **2014**, *485*, 172–180.
52. Patel, M.; Jindal, T.K.; Pant, K.K. Kinetic Study of Steam Reforming of Ethanol on Ni-Based Ceria-Zirconia Catalyst. *Ind. Eng. Chem. Res.* **2013**, *52*, 15763–15771.
53. Beretta, A.; Donazzi, A.; Groppi, G.; Forzatti, P.; dal Santo, V.; Sordelli, L.; de Grandi, V.; Psaro, R. Testing in annular micro-reactor and characterization of supported Rh nanoparticles for the catalytic partial oxidation of methane: Effect of the preparation procedure. *Appl. Catal. B* **2008**, *83*, 96–109.
54. Farrauto, R.J.; Bartholomew, C.H. *Fundamentals of Industrial Catalytic Processes*, 2nd ed.; John Wiley & Sons: Hoboken, NJ, USA, 2005.
55. Jiaxiu, G.; Zhonghua, S.; Dongdong, W.; Huaqiang, Y.; Maochu, G.; Yaoqiang, C. Study of Pt–Rh/CeO_2-ZrO_2-M_xO_y (M = Y, La)/Al_2O_3 three-way catalysts. *Appl. Surf. Sci.* **2013**, *273*, 527–535.
56. Kirszensztejn, P.; Wachowski, L.; Szymkowiak, A.; Hofman, M.; Przekop, R. Physicochemical and surface properties of alumina modified with rare earth oxides, III. Dispersion of supported platinum. *React. Kinet. Catal. Lett.* **2004**, *81*, 189–195.
57. Machocki, A.; Denis, A.; Grzegorczyk, W.; Gac, W. Nano- and micro-powder of zirconia and ceria-supported cobalt catalysts for the steam reforming of bio-ethanol. *Appl. Surf. Sci.* **2010**, *256*, 5551–5558.
58. Parres-Esclapez, S.; Such-Basañez, I.; Illán-Gómez, M.J.; Salinas-Martínez de Lecea, C.; Bueno-López, A. Study by isotopic gases and *in situ* spectroscopies (DRIFTS, XPS and Raman) of the N_2O decomposition mechanism on Rh/CeO_2 and Rh/γ-Al_2O_3 catalysts. *J. Catal.* **2010**, *276*, 390–401.

59. Zhu, X.; Xie, Y.; Liu, C.J.; Zhang, Y. Stability of Pt particles on ZrO_2 support during partial oxidation of methane: DRIFT studies of adsorbed CO. *J. Mol. Catal. A* **2008**, *282*, 67–73.
60. Sheng, P.Y.; Chiu, W.W.; Yee, A.; Morrison, S.J.; Idriss, H. Hydrogen production from ethanol over bimetallic Rh-M/CeO_2 (M = Pd or Pt). *Catal. Today* **2007**, *129*, 313–321.
61. Kaila, R.K.; Gutiérrez, A.; Slioor, R.; Kemell, M.; Leskelä, M.; Krause, A.O.I. Zirconia-supported bimetallic RhPt catalysts: Characterization and testing in autothermal reforming of simulated gasoline. *Appl. Catal. B* **2008**, *84*, 223–232.
62. Bueno-López, A.; Such-Basáñez, I.; Salinas-Martínez de Lecea, C. Stabilization of active Rh_2O_3 species for catalytic decomposition of N_2O on La-, Pr-doped CeO_2. *J. Catal.* **2006**, *244*, 102–112.
63. Avgouropoulos, G.; Papavasiliou, J.; Ioannides, T. Hydrogen production from methanol over combustion-synthesized noble metal/ceria catalysts. *Chem. Eng. J.* **2009**, *154*, 274–280.
64. Kugai, J.; Subramani, V.; Song, C.; Engelhard, M.; Chin, Y. Effects of nanocrystalline CeO_2 supports on the properties and performance of Ni-Rh bimetallic catalyst for oxidative steam reforming of ethanol. *J. Catal.* **2006**, *238*, 430–440.
65. Liu, H.-H.; Wang, Y.; Jia, A.-P.; Wang, S.-Y.; Luo, M.-F.; Lu, J.-Q. Oxygen vacancy promoted CO oxidation over Pt/CeO_2 catalysts: A reaction at Pt-CeO_2 interface. *Appl. Surf. Sci.* **2014**, *314*, 725–734.
66. Gu, D.M.; Chu, Y.Y.; Wang, Z.B.; Jiang, Z.Z.; Yin, G.-P.; Liu, Y. Methanol oxidation on Pt/CeO_2-C electrocatalyst prepared by microwave-assisted ethylene glycol process. *Appl. Catal. B* **2011**, *102*, 9–18.
67. Özkara-Aydınoğlu, Ş.; Özensoy, E.; Aksoylu, A.E. The effect of impregnation strategy on methane dry reforming activity of Ce promoted Pt/ZrO_2. *Int. J. Hydrogen Energy* **2009**, *34*, 9711–9722.
68. Holgado, J.P.; Munuera, G. XPS/TPR study of the reducibility of M/CeO_2 catalysts (M = Pt, Rh): Does junction effect theory apply? *Stud. Surf. Sci. Catal.* **1995**, *96*, 109–122.
69. Tanabe, T.; Morikawa, A.; Hatanaka, M.; Takahashi, N.; Nagai, Y.; Sato, A.; Kuno, O.; Suzuki, H.; Shinjoh, H. The interaction between supported Rh- and Nd_2O_3-enriched surface layer on ZrO_2 for Rh sintering suppression. *Catal. Today* **2012**, *184*, 219–226.
70. Chen, X.; Li, H.; Dai, W.; Wang, J.; Ran, Y.; Qiao, M. Selective hydrogenation of cinnamaldehyde to cinnamyl alcohol over the Co-La-B/SiO_2 amorphous catalyst and the promoting effect of La-dopant. *Appl. Catal. A* **2003**, *253*, 359–369.
71. Silva, A.M.; Costa, L.O.O.; Barandas, A.P.M.G.; Borges, L.E.P.; Mattos, L.V.; Noronha, F.B. Effect of the metal nature on the reaction mechanism of the partial oxidation of ethanol over CeO_2-supported Pt and Rh catalysts. *Catal. Today* **2008**, *133–135*, 755–761.
72. Calles, J.; Carrero, A.; Vizcaíno, A.; Lindo, M. Effect of Ce and Zr Addition to Ni/SiO_2 Catalysts for Hydrogen Production through Ethanol Steam Reforming. *Catalysts* **2015**, *5*, 58–76.
73. Aghazadeh, M.; Arhami, B.; Malek Barmi, A.-A.; Hosseinifard, M.; Gharailou, D.; Fathollahi, F. $La(OH)_3$ and La_2O_3 nanospindles prepared by template-free direct electrodeposition followed by heat-treatment. *Mater. Lett.* **2014**, *115*, 68–71.
74. Divins, N.J.; López, E.; Rodríguez, Á.; Vega, D.; Llorca, J. Bio-ethanol steam reforming and autothermal reforming in 3-μm channels coated with RhPd/CeO_2 for hydrogen generation. *Chem. Eng. Process. Process Intensif.* **2013**, *64*, 31–37.

75. Sahoo, D.; Vajpai, S.; Patel, S.; Pant, K. Kinetic modeling of steam reforming of ethanol for the production of hydrogen over Co/Al_2O_3 catalyst. *Chem. Eng. J.* **2007**, *125*, 139–147.
76. Mondal, T.; Pant, K.K.; Dalai, A.K. Catalytic oxidative steam reforming of bio-ethanol for hydrogen production over Rh promoted Ni/CeO_2-ZrO_2 catalyst. *Int. J. Hydrogen Energy* **2015**, *40*, 2529–2544.
77. Yuan, G.; Keane, M.A. Liquid phase hydrodechlorination of chlorophenols over Pd/C and Pd/Al_2O_3: A consideration of HCl/catalyst interactions and solution pH effects. *Appl. Catal. B* **2004**, *52*, 301–314.
78. Krishnankutty, N.; Vannice, M.A. The Effect of Pretreatment on Pd/C Catalysts I. Adsorption and Absorption Properties. *J. Catal.* **1995**, *155*, 312–326.
79. Davis, M.E.; Davis, R.J. *Fundamentals of Chemical Reaction Engineering*; McGraw-Hill Higher: Columbus, OH, USA, 2003; Volume 4.